INSTITUTE OF PHYSICS PUBLISHING PHYSIOLOGICAL MEASUREMENT

Physiol. Meas. **26** (2005) S279–S288 doi:10.1088/0967-3334/26/2/026

Electrical conductivity images of biological tissue phantoms in MREIT

Suk Hoon Oh[1], Byung Il Lee[1], Eung Je Woo[1], Soo Yeol Lee[1], Tae-Seong Kim[1], Ohin Kwon[2] and Jin Keun Seo[3]

[1] College of Electronics and Information, Kyung Hee University, Korea
[2] Department of Mathematics, Konkuk University, Korea
[3] Department of Mathematics, Yonsei University, Korea

E-mail: oikwon@konkuk.ac.kr

Received 18 September 2004, accepted for publication 4 January 2005
Published 29 March 2005
Online at stacks.iop.org/PM/26/S279

Abstract

We present cross-sectional conductivity images of two biological tissue phantoms. Each of the cylindrical phantoms with both diameter and height of 140 mm contained chunks of biological tissues such as bovine tongue and liver, porcine muscle and chicken breast within a conductive agar gelatin as the background medium. We attached four recessed electrodes on the sides of the phantom with equal spacing among them. Injecting current pulses of 480 or 120 mA ms into the phantom along two different directions, we measured the z-component B_z of the induced magnetic flux density $\mathbf{B} = (B_x, B_y, B_z)$ with a magnetic resonance electrical impedance tomography (MREIT) system based on a 3.0 T MRI scanner. Using the harmonic B_z algorithm, we reconstructed cross-sectional conductivity images from the measured B_z data. Reconstructed images clearly distinguish different tissues in terms of both their shapes and conductivity values. In this paper, we experimentally demonstrate the feasibility of the MREIT technique in producing conductivity images of different biological soft tissues with a high spatial resolution and accuracy when we use a sufficient amount of the injection current.

Keywords: MREIT, conductivity image, biological tissue, magnetic flux density

1. Introduction

Information about electrical conductivity distribution inside biological tissues is of significant importance in many biomedical applications, such as modeling of tissues to investigate action potential propagations, estimation of therapeutic current distributions during electrical stimulations and monitoring of physiological functions (Sersa *et al* 1997). In combinatory

studies of fMRI with other brain mapping modalities, such as EEG and MEG, information on the conductivity distribution inside the brain is essential to precisely localize activated regions (Lazeyras *et al* 2001).

Conductivity image reconstruction has been the active research goal of electrical impedance tomography (EIT) since the early 1980s (Webster 1990, Boone *et al* 1997, Saulnier *et al* 2001). Lately, magnetic resonance electrical impedance tomography (MREIT) has been suggested to overcome the ill-posedness of the image reconstruction problem in EIT (Zhang 1992, Woo *et al* 1994, Ider and Birgul 1998, Kwon *et al* 2002, Khang *et al* 2002, Lee *et al* 2003a, Birgul *et al* 2003, Ider *et al* 2003, Hasanov *et al* 2004, Joy 2004). The key idea is to utilize the internal magnetic flux density data measured by a MRI scanner. When we inject current through a pair of surface electrodes into an electrically conducting subject such as the human body, it induces voltage, current density and magnetic flux density distributions. These distributions are determined by the geometry, electrode configuration and conductivity distribution of the subject (Lee *et al* 2003b). Unlike EIT where we are limited by the surface measurements of the current–voltage data, MREIT utilizes the internal magnetic flux density produced by the injection current. Several conductivity image reconstruction algorithms have been developed based on the measurement of only one component B_z of the magnetic flux density $\mathbf{B} = (B_x, B_y, B_z)$ (Seo *et al* 2003b, 2003a, Oh *et al* 2003, Park *et al* 2004b, 2004a, Ider and Onart 2004). These algorithms are based only on B_z since the subject inside the MRI scanner must be rotated in order to measure B_x or B_y (Scott *et al* 1991, 1992). Here, we assume that the direction of the main magnetic field of the MRI scanner is parallel to the z-axis.

Previous studies in MREIT showed that cross-sectional conductivity images with much improved accuracy and spatial resolution are obtainable using numerical simulation methods (Seo *et al* 2003b, 2003a, Oh *et al* 2003, Park *et al* 2004b, 2004a). Preliminary experimental work also showed the feasibility of the technique (Oh *et al* 2003, 2004, Hasanov *et al* 2004, Woo *et al* 2004). The purpose of this paper is to validate the method using phantoms including biological tissues. The results described in this paper suggest a possibility of *in vivo* animal imaging with the MREIT technique before we apply it to human subjects.

2. Methods

2.1. Conductivity image reconstruction problem in MREIT

The conductivity image reconstruction problem in MREIT has been described in several previous works based on the assumption that only B_z is measured without rotating the subject (Seo *et al* 2003b, 2003a, Oh *et al* 2003, Park *et al* 2004b, 2004a, Ider and Onart 2004). In this section, we briefly summarize the problem and describe one of the proposed image reconstruction algorithms.

We denote a three-dimensional electrically conducting subject as Ω with its boundary $\partial\Omega$. The conductivity distribution in Ω is denoted as σ. In this paper, the conductivity is assumed to be isotropic. Attaching a pair of surface electrodes on $\partial\Omega$, we inject current I into the subject. Then, the voltage u is a solution of the following boundary value problem:

$$\begin{cases} \nabla \cdot (\sigma \nabla u) = 0 & \text{in} \quad \Omega \\ -\sigma \nabla u \cdot \nu = g & \text{on} \quad \partial\Omega \end{cases} \tag{1}$$

where ν is the unit outward normal vector to the boundary $\partial\Omega$, and g is the corresponding Neumann boundary condition due to the injection current I.

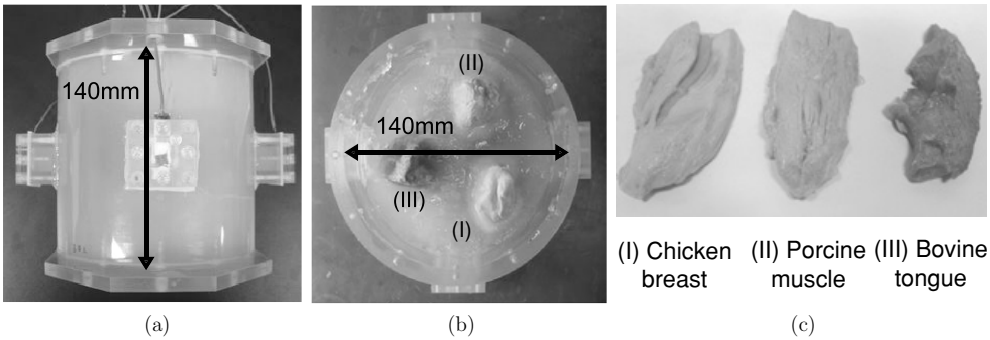

Figure 1. Tissue phantom: (a) side view, (b) top view and (c) chunks of biological tissues before being placed inside the phantom.

According to the Biot–Savart law, the z-component of the magnetic flux density B_z inside Ω can be represented as

$$B_z(\mathbf{r}) = \frac{\mu_0}{4\pi} \int_\Omega \frac{\sigma(\mathbf{r}')\left[(y-y')\frac{\partial u(\mathbf{r}')}{\partial x} - (x-x')\frac{\partial u(\mathbf{r}')}{\partial y}\right]}{|\mathbf{r}-\mathbf{r}'|^3} \, \mathrm{d}\mathbf{r}' + B_z^I(\mathbf{r}) \tag{2}$$

where $\mathbf{r} = (x, y, z) \in \Omega$, $\mathbf{r}' = (x', y', z') \in \Omega$ and B_z^I is the magnetic flux density due to the current I along external lead wires. In MREIT experiments, we measure this B_z using a MRI scanner. From (1) and (2), we observe that B_z can be computed from g and σ. Conversely, the relation from g to B_z contains some information of the conductivity distribution σ. In MREIT, we try to reconstruct an image of σ from the relationship between multiple injection currents I^j with $j = 1, \ldots, N$ and the corresponding B_z^j via the governing equations (1) and (2).

Three different conductivity image reconstruction algorithms have been recently suggested based on the relations in (1) and (2). They are the harmonic B_z algorithm (Seo *et al* 2003b, Oh *et al* 2003), variational gradient B_z algorithm (Park *et al* 2004b) and gradient B_z decomposition algorithm (Park *et al* 2004a). In this paper, we choose to use the harmonic B_z algorithm that is based on the following identity:

$$\begin{bmatrix} \frac{\partial u^1}{\partial y} & -\frac{\partial u^1}{\partial x} \\ \vdots & \vdots \\ \frac{\partial u^N}{\partial y} & -\frac{\partial u^N}{\partial x} \end{bmatrix} \begin{bmatrix} \frac{\partial \sigma}{\partial x} \\ \frac{\partial \sigma}{\partial y} \end{bmatrix} = \frac{1}{\mu_0} \begin{bmatrix} \nabla^2 B_z^1 \\ \vdots \\ \nabla^2 B_z^N \end{bmatrix} \tag{3}$$

for each position inside the subject Ω. Seo *et al* (2003b) and Oh *et al* (2003) described the details of the algorithm. Since the primary purpose of this paper is to experimentally validate the MREIT techniques in terms of reconstructing conductivity images of biological tissues, we will use only the harmonic B_z algorithm in this paper though there are others available.

2.2. Biological tissue phantom

Figure 1 shows one of the two three-dimensional phantoms containing different biological tissues. Both diameter and height of the cylindrical acrylic phantom were 140 mm. After placing chunks of biological tissues inside the empty phantom, we filled it with agar gelatin (1 g l^{-1} $CuSO_4$, 3.125 g l^{-1} NaCl, 7 g l^{-1} agar). We used four different biological tissues obtained from a local grocery store and they are bovine liver and tongue, porcine muscle and

Table 1. Measured (σ_M) and reconstructed (σ_R) conductivity values of five different objects inside tissue phantoms. Reconstructed conductivity values are shown in mean ± standard deviation. We measured the conductivity values after the experiments using the four-electrode method with an impedance analyzer.

Object	σ_M (S m^{-1})	σ_R (S m^{-1})
Chicken breast	0.55–0.60	0.52 ± 0.03–0.54 ± 0.04
Bovine tongue	0.36–0.41	0.44 ± 0.04
Porcine muscle	0.55–0.64	0.59 ± 0.07
Bovine liver	0.69	0.55 ± 0.14
Agar gelatin	0.76	0.73 ± 0.02

chicken breast. The first phantom contained bovine liver, porcine muscle and chicken breast. In the second phantom, we placed bovine tongue, porcine muscle and chicken breast with different sizes and shapes.

On the middle of the cylindrical surface of the tissue phantom, four recessed electrode assemblies were attached with equal spacing among them to inject current into the phantom. Using recessed electrodes, we can avoid many troubles caused by the conventional metal electrodes directly attached on the surface of the subject (Lee *et al* 2003a, Oh *et al* 2003). The size of each recessed electrode assembly was $20 \times 20 \times 30$ mm^3, and the electrode was made of silver with the size of 10×20 mm^2. In order to compare the accuracy of the reconstructed conductivity images, we measured the conductivity of each tissue after the experiments with an impedance analyzer (4192A, Agilent Technologies, USA) using the four-electrode method. Table 1 shows the measured conductivity values of the tissues and agar gelatin.

2.3. MREIT experiments

After placing the phantom inside our MREIT system based on a 3.0 T MRI scanner (Magnum 3.0, Medinus Inc., Korea), we injected current I^1 between one pair of electrodes facing each other. To measure the induced internal magnetic flux density B_z^1, the pulse sequence shown in figure 2 was used with the multi-slice gradient echo imaging technique. The amount of the injection current was 480 mA ms with the pulse width of $T_c = 10$ ms. The slice thickness was 3 mm with no slice gaps, TR was 1000 ms and TE was 14 ms. The number of axial slices was eight and therefore the imaging region was a cylindrical section of 24 mm length at the middle of the phantom. After acquiring eight slices of B_z^1 images for I^1, another current I^2 of the same amount was injected through the other pair of electrodes to obtain the corresponding B_z^2 images. During each current injection, we measured the voltage difference between the other pair of electrodes that were not used for the current injection. With respect to these measured voltage data, the reconstructed conductivity values were scaled to absolute conductivity values as described in Lee *et al* (2003a) and Oh *et al* (2003). For one of the phantoms, we repeated the same experiment using a different amount of the injection current of 120 mA ms.

Phase images with the matrix size of 128×128 were calculated from the k-space data. Field-of-view (FOV) was 200×200 mm^2 and pixel size was 1.56×1.56 mm^2. We converted unwrapped phase images into magnetic flux density images of B_z^1 and B_z^2 by an appropriate scaling (Khang *et al* 2002, Lee *et al* 2003a, Oh *et al* 2003).

3. Results

Figures 3(a) and (b) show the MR magnitude images of the phantoms at the middle imaging slices. In figure 3(a), we can see air bubbles around large blood vessels in the bovine liver.

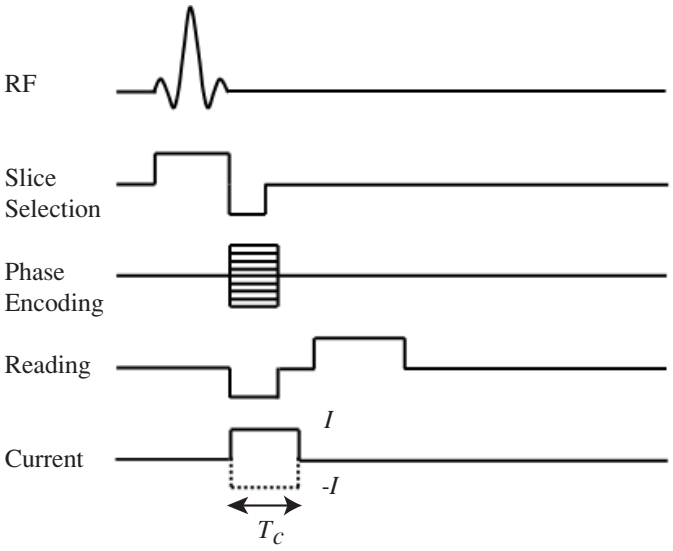

Figure 2. Gradient echo pulse sequence with synchronized injection current pulses.

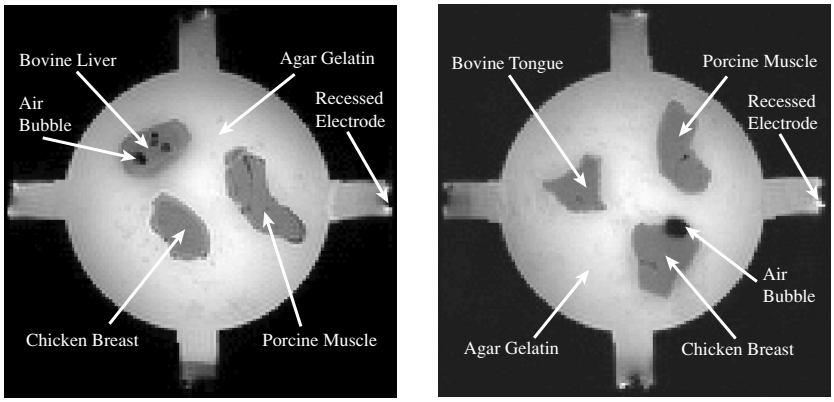

Figure 3. MR magnitude images of two tissue phantoms at the middle imaging slice.

Figure 3(b) shows a bigger air bubble near the chicken breast that was produced when the agar gelatin was poured into the phantom. Figures 4(a) and (b) are the measured images of B_z^1 and B_z^2 from the phantom in figure 3(a). Figures 4(c) and (d) are the measured images of B_z^1 and B_z^2 for the phantom in figure 3(b).

Figure 5(b) is the reconstructed cross-sectional conductivity image corresponding to the MR magnitude image in figure 3(a). We showed the MR magnitude image in figure 5(a) again for easier comparison. Figures 6(a) and (b) show the corresponding images for the phantom in figure 3(b). Figure 6(c) is the reconstructed conductivity image using 120 mA ms injection current. Compared with the conductivity image in figure 6(b) using 480 mA ms, it is more noisy since the smaller injection current produced weaker B_z^1 and B_z^2 signals, and the amount of noise was almost same due to the same pulse sequence. The computation time to reconstruct each conductivity image was about 55 min with five iterations of the harmonic B_z

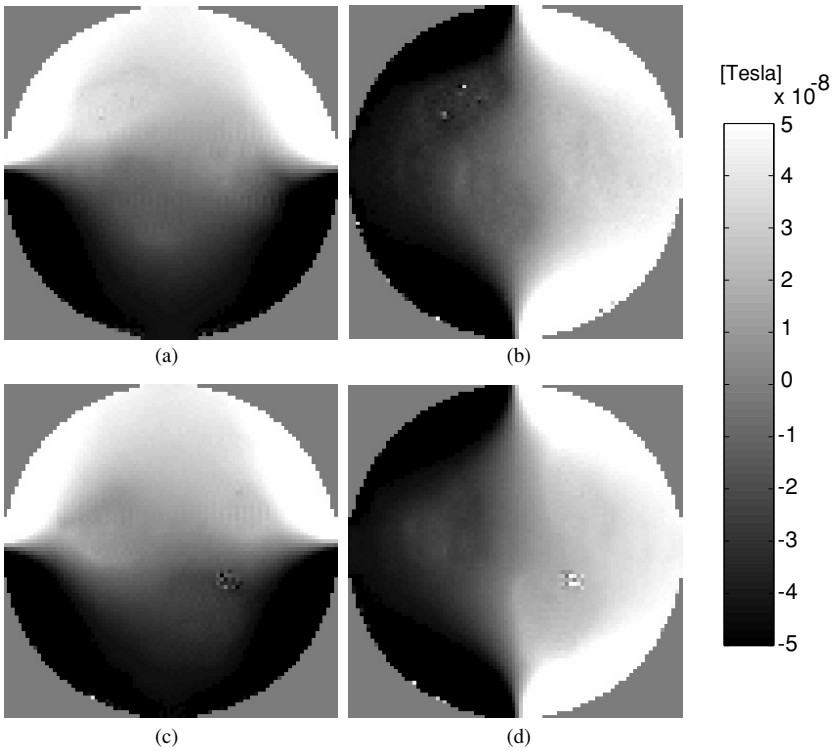

Figure 4. Measured images of (a) B_z^1 and (b) B_z^2 for the phantom in figure 3(a) at the middle imaging slice. Parts (c) and (d) are the corresponding images of B_z^1 and B_z^2 for the phantom in figure 3(b). The injection current was 480 mA ms.

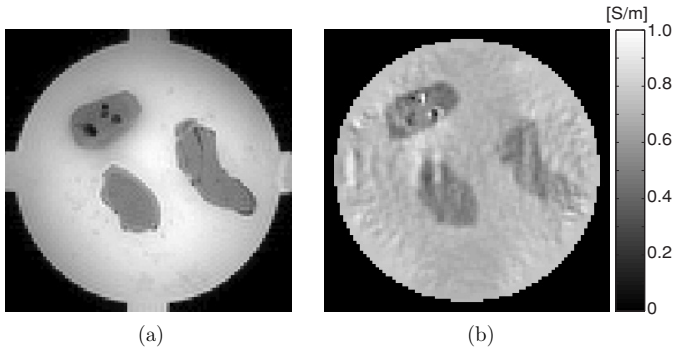

Figure 5. Images from the phantom in figure 3(a) at the middle imaging slice: (a) MR magnitude image and (b) reconstructed conductivity image with the injection current of 480 mA ms.

algorithm using a PC (Pentium IV, 1 GHz main clock and 2 MB RAM). Table 1 shows means and standard deviations of the reconstructed conductivity values inside different tissue objects in figures 5(b) and 6(b).

Figure 7 shows three reconstructed conductivity images from the top, middle and bottom slice of the phantom in figure 3(b). The distance between the top and bottom slice was 21 mm. We can observe that the reconstructed conductivity images are different for each slice. This

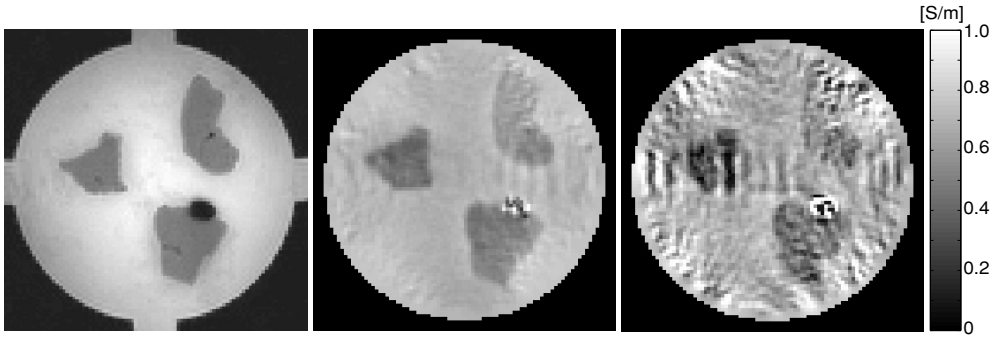

Figure 6. Images from the phantom in figure 3(b) at the middle imaging slice: (a) MR magnitude image, (b) reconstructed conductivity image with 480 mA ms injection current and (c) with 120 mA ms injection current.

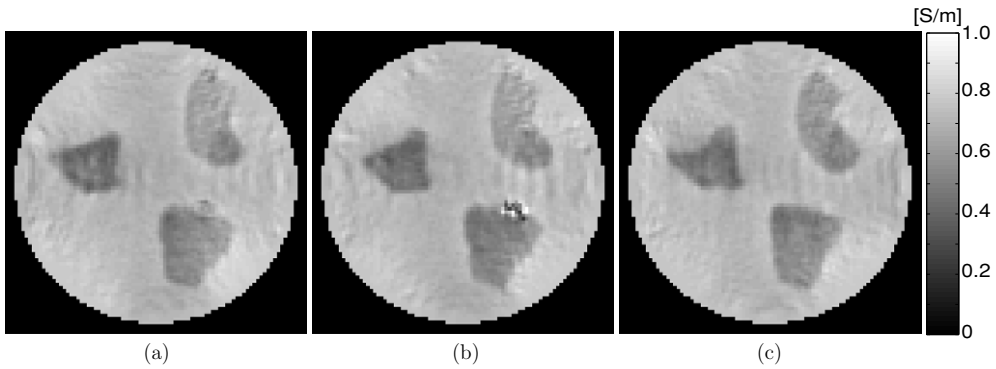

Figure 7. Reconstructed conductivity images from the phantom in figure 3(b) at the (a) top, (b) middle and (c) bottom imaging slice. The distance between the top and bottom slice was 21 mm and the amount of the injection current was 480 mA ms.

indicates that we can reconstruct conductivity images of a three-dimensional subject with variations in the z-direction.

4. Discussion

We have demonstrated that conductivity images of different biological soft tissues with relatively small contrast can be successfully reconstructed. Unlike the early MREIT techniques (Kwon *et al* 2002, Khang *et al* 2002, Lee *et al* 2003a, Birgul *et al* 2003, Ider *et al* 2003) where orthogonal rotations of the subject inside the MRI scanner were required, the method used in this paper is based on the measurement of only one component B_z of the induced magnetic flux density $\mathbf{B} = (B_x, B_y, B_z)$. This B_z-based MREIT significantly improves the applicability of the technique by eliminating the subject rotation procedure. Using recessed electrodes was also found to be quite effective since they allow us to obtain clear magnetic flux density images inside the subject near the electrodes as shown in figures 4.

Figure 3 shows that there were air bubbles inside the phantoms. Since we could not get MR signals from the regions of the air bubbles, we can observe that the B_z signals within those

regions were very noisy from the B_z images in figure 4. This produced noisy conductivity values there in the reconstructed images as shown in figures 5, 6 and 7. It is also possible that the reconstructed conductivity values near the air bubbles could have been underestimated since air bubbles are insulators. Table 1 shows a bigger difference between the measured and reconstructed conductivity values inside the bovine liver. We speculate that air bubbles inside the bovine liver could have caused this noticeably larger error. Since MR magnitude images are always available in MREIT, in our future study, we should utilize this *a priori* information to better handle this kind of artifacts.

The amount of the injection current used in this study is too large to be applied for human subjects. The biggest hurdle in reducing this amount is the presence of Gaussian random noise in measured magnetic flux density images (Scott *et al* 1992). As shown in figures 6(b) and (c), reducing the amount of the injection current from 480 mA ms to 120 mA ms degrades the image quality. In order to reduce the injection current without much deteriorating the image quality, we must devise different ways to reduce the noise level. For a given subject with a certain size and electrode configuration, the amount of the injection current and pulse sequence are major factors determining the signal-to-noise ratio (SNR) in measured B_z images. Noting that the magnitude of the induced magnetic flux density B_z is proportional to the amplitude of the injection current pulse and the noise level in B_z is inversely proportional to the duration of the pulse, we need to investigate new MREIT pulse sequences.

Incorporating efficient denoising techniques into conductivity image reconstruction algorithms are also promising. Lately, Kim *et al* (2004) suggested a new denoising technique for MREIT, and it is based on diffusion partial differential equation utilizing MR magnitude image as *a priori* information. Our future studies in MREIT should be focused on reducing the amount of the injection current by developing new MREIT pulse sequences, better electrode configurations, denoising techniques and others. Conductivity imaging in a reduced field of view or a region of interest is also worth pursuing.

The different biological tissues obtained from a local grocery store showed a very small degree of anisotropy in terms of the measured conductivity values using the impedance analyzer. Since the harmonic B_z algorithm used in this paper ignores the anisotropy, the reconstructed conductivity images given in figures 5, 6 and 7 represent the equivalent isotropic conductivity values, hence, they may contain a small amount of errors. In MREIT using a low-frequency injection current, the anisotropy of tissue conductivity could be a definite problem in *in vivo* experimental studies since muscular and neuronal tissues show a strong anisotropy. Even though Seo *et al* (2004) proposed an anisotropic conductivity image reconstruction algorithm in MREIT, further analysis and studies on its stability against measurement noise are required. For the time being, the proposed technique can still be applied to find equivalent isotropic conductivity images.

5. Conclusion

This paper presents cross-sectional conductivity images of biological soft tissues using the MREIT technique. The pixel size was 1.56×1.56 mm^2 and there were 90×90 pixels in each conductivity image. To the best of our knowledge, this kind of spatial resolution has never been achieved in other conductivity imaging techniques. In addition, the reconstructed conductivity values were found to be quite close to those measured by using an impedance analyzer.

One of the most important technical problems to be solved in MREIT is the reduction of the amount of the injection current: in this study, it was 48 mA $\times$ 10 ms. With 12 mA $\times$ 10 ms injection current, the image quality significantly deteriorated. Reducing the amount below the

level enforced by the safety regulation would be the biggest challenge in MREIT for human imaging. Our studies in the near future include efficient denoising techniques to improve the signal-to-noise ratio in measured B_z data and numerous ways to utilize *a priori* information that can be found from MR magnitude images. We plan to apply the technique to animal imaging before we try it on human subjects.

The results described in this paper suggest that MREIT is feasible in reconstructing cross-sectional conductivity images with enough spatial resolution and accuracy for many applications in biology, chemistry and medicine. As we make more progress in the MREIT research, we will be looking for different application areas.

Acknowledgments

This work was supported by the grant R11-2002-103 from Korea Science and Engineering Foundation (KOSEF), and O Kwon was supported by Korea Research Foundation Grant (KRF-2002-003-C00018).

References

Birgul O, Eyuboglu B M and Ider Y Z 2003 Current constrained voltage scaled reconstruction (CCVSR) algorithm for MR-EIT and its performance with different probing current patterns *Phys. Med. Biol.* **48** 653–71

Boone K, Barber D and Brown B 1997 Imaging with electricity: report of the European concerted action on impedance tomography *J. Med. Eng. Technol.* **21** 201–32

Hasanov K F, Ma A W, Yoon R S, Nachman A I and Joy M L 2004 A new approach to current density impedance imaging *Proc. 26th Annu. Int. Conf. IEEE EMBS (San Francisco, CA, USA)* pp 1321–4

Ider Y Z and Birgul O 1998 Use of the magnetic field generated by the internal distribution of injected currents for electrical impedance tomography (MR-EIT) *Elektrik* **6** 215–25

Ider Y Z and Onart S 2004 Algebraic reconstruction for 3D MR-EIT using one component of magnetic flux density *Physiol. Meas.* **25** 281–94

Ider Y Z, Onart S and Lionheart W R B 2003 Uniqueness and reconstruction in magnetic resonance-electrical impedance tomography (MR-EIT) *Physiol. Meas.* **24** 591–604

Joy M L 2004 MR current density and conductivity imaging: the state of the art *Proc. 26th Annu. Int. Conf. IEEE EMBS (San Francisco, CA, USA)* pp 5315–9

Khang H S, Lee B I, Oh S H, Woo E J, Lee S Y, Cho M H, Kwon O, Yoon J R and Seo J K 2002 J-substitution algorithm in magnetic resonance electrical impedance tomography (MREIT): phantom experiments for static resistivity images *IEEE Trans. Med. Imaging* **21** 695–702

Kim T S, Lee B I, Lee S H, Seo J K, Kwon O and Woo E J 2004 Diffusion PDE-based denoising technique for magnetic resonance electrical impedance tomography *Proc. 26th Annu. Int. Conf. IEEE EMBS (San Francisco, CA, USA)* pp 1036–9

Kwon O, Woo E J, Yoon J R and Seo J K 2002 Magnetic resonance electrical impedance tomography (MREIT): simulation study of J-substitution algorithm *IEEE Trans. Biomed. Eng.* **48** 160–7

Lazeyras F, Zimine I, Blanke O, Perrig S H and Seeck M 2001 Functional MRI with simultaneous EEG recording: feasibility and application to motor and visual activation *J. Magn. Reson. Imaging* **13** 943–8

Lee B I, Oh S H, Woo E J, Lee S Y, Cho M H, Kwon O, Seo J K and Baek W S 2003a Static resistivity image of a cubic saline phantom in magnetic resonance electrical impedance tomography (MREIT) *Physiol. Meas.* **24** 579–89

Lee B I, Oh S H, Woo E J, Lee S Y, Cho M H, Kwon O, Seo J K, Lee J Y and Baek W S 2003b Three-dimensional forward solver and its performance analysis in magnetic resonance electrical impedance tomography (MREIT) using recessed electrodes *Phys. Med. Biol.* **48** 1971–86

Oh S H, Lee B I, Park T S, Lee S Y, Woo E J, Cho M H, Kwon O and Seo J K 2004 Magnetic resonance electrical impedance tomography at 3 Tesla field strength *Mag. Reson. Med.* **51** 1292–6

Oh S H, Lee B I, Woo E J, Lee S Y, Cho M H, Kwon O and Seo J K 2003 Conductivity and current density image reconstruction using harmonic B_z algorithm in magnetic resonance electrical impedance tomography *Phys. Med. Biol.* **48** 3101–16

Park C, Kwon O, Woo E J and Seo J K 2004a Electrical conductivity imaging using gradient B_z decomposition algorithm in magnetic resonance electrical impedance tomography (MREIT) *IEEE Trans. Med. Imaging* **23** 388–94

Park C, Park E J, Woo E J, Kwon O and Seo J K 2004b Static conductivity imaging using variational gradient B_z algorithm in magnetic resonance electrical impedance tomography *Physiol. Meas.* **25** 257–69

Saulnier G J, Blue R S, Newell J C, Isaacson D and Edic P M 2001 Electrical impedance tomography *IEEE Signal Process. Mag.* **18** 31–43

Scott G C, Joy M L G, Armstrong R L and Henkelman R M 1991 Measurement of nonuniform current density by magnetic resonance *IEEE Trans. Med. Imaging* **10** 362–74

Scott G C, Joy M L G, Armstrong R L and Hankelman R M 1992 Sensitivity of magnetic resonance current density imaging *J. Magn. Reson.* **97** 235–54

Seo J K, Kwon O, Lee B I and Woo E J 2003a Reconstruction of current density distributions in axially symmetric cylindrical sections using one component of magnetic flux density: computer simulation study *Physiol. Meas.* **24** 565–77

Seo J K, Pyo H C, Park C J, Kwon O and Woo E J 2004 Image reconstruction of anisotropic conductivity tensor distribution in MREIT: computer simulation study *Phys. Med. Biol.* **49** 4371–82

Seo J K, Yoon J R, Woo E J and Kwon O 2003b Reconstruction of conductivity and current density images using only one component of magnetic field measurements *IEEE Trans. Biomed. Eng.* **50** 1121–4

Sersa I, Beravs K, Dodd N J F, Zhao S, Miklavcic D and Demsar F 1997 Electric current density imaging of mice tumors *Magn. Reson. Med.* **37** 404–9

Webster J G (ed) 1990 *Electrical Impedance Tomography* (Bristol, UK: Adam Hilger)

Woo E J, Lee S Y and Mun C W 1994 Impedance tomography using internal current density distribution measured by nuclear magnetic resonance *SPIE* **2299** 377–85

Woo E J, Lee S Y, Seo J K, Kwon O, Oh S H and Lee B I 2004 Conductivity images of biological tissue phantoms using a 3.0 Tesla MREIT system *Proc. 26th Annu. Int. Conf. IEEE EMBS (San Francisco, CA, USA)* pp 1287–9

Zhang N 1992 Electrical impedance tomography based on current density imaging *MS Thesis* Department of Electrical Engineering, University of Toronto, Toronto, Canada